Research Square

Preprints are preliminary reports that have not undergone peer review.
They should not be considered conclusive, used to inform clinical practice,
or referenced by the media as validated information.

Integrated metabolomic and proteomic analyses reveal the regulatory mechanism of H-2-168 against Echinococcus granulosus infection in mice

Yixueying Ma
Xinjiang Medical University
Qinwei Xu
Xinjiang Medical University
Yujie Huang
Xinjiang Medical University
Jinxin Li
Xinjiang Medical University
Haoyuan Xu
People's Hospital of Bayingolin Mongolian Autonomous Prefecture
Huijing Gao
Xinjiang Medical University
Liang Teng
tl750212@126.com

Xinjiang Medical University

Research Article

Keywords: Cystic echinococcosis, Echinococcus granulosus, Harmine derivative H-2-168, Metabolomics, Proteomics, LC-MS/MS

Posted Date: July 1st, 2026

DOI: https://doi.org/10.21203/rs.3.rs-10129376/v1

License: This work is licensed under a Creative Commons Attribution 4.0 International License.
Read Full License

Additional Declarations: No competing interests reported.

Abstract

Background

Cystic echinococcosis (CE), a severe zoonotic parasitic disease caused by *Echinococcus granulosus (E. granulosus)*, causes hepatic injury, inflammatory infiltration and metabolic disorders, severely threatening human health and animal husbandry. Harmine derivative H-2-168 exhibits potent in vitro anti-echinococcal activity, yet its in vivo intervention mechanism, particularly the changes in differential metabolites and proteins in CE-infected livers, remains unclear.

Methods

We employed liquid chromatography-tandem mass spectrometry (LC-MS/MS)-based metabolomics coupled with proteomics to systematically investigate the intervention effects and molecular mechanisms of H-2-168 in *E. granulosus*-infected mice.

Results

Metabolomics analysis identified 87 significantly altered metabolites (54 upregulated, 33 downregulated) in the H-2-168 group, including upregulated α-linolenic acid and ABC transporters, and downregulated creatinine and all-trans retinoic acid. These metabolites were enriched in D-amino acid metabolism, linoleic acid metabolism, peroxisome proliferator-activated receptor (PPAR) signaling, and glutathione metabolism pathways. Proteomics revealed 238 differentially expressed proteins (113 upregulated, 125 downregulated), primarily involved in metabolic regulation, inflammation, signal transduction, oxidative stress, and DNA repair. Integrated multi-omics analysis highlighted significant changes in tryptophan metabolism, sphingolipid metabolism, and ferroptosis pathways, with 8 key signaling pathways, 9 core proteins, and 18 pivotal metabolites identified, forming a complex regulatory network.

Conclusions

H-2-168 alleviates CE-induced hepatic injury by modulating hepatic metabolic pathways and related protein expression. This study provides an experimental basis for elucidating the mechanism of H-2-168 and offers novel targets for CE treatment.

Background

Cystic echinococcosis (CE), also known as hydatid disease, is a severe zoonotic parasitic disease caused by the larval stage of *Echinococcus granulosus (E. granulosus)* parasitizing the internal organs of mammals. It is characterized by a global distribution [1, 2]. *E. granulosus* belongs to the family Taeniidae

(phylum Platyhelminthes, class Cestoda, order Cyclophyllidea) [3]. Its life cycle involves obligatory alternating parasitism between definitive hosts (e.g., domestic dogs, wolves, and other canids) and intermediate hosts (e.g., humans, cattle, and sheep). Adult tapeworms reside in the intestines of definitive hosts, causing only mild intestinal parasitism. In contrast, the larval stage (protoscoleces), which parasitizes the liver, lungs, and other organs of intermediate hosts, forms hydatid cysts, leading to organ damage [4, 5].

According to the World Health Organization (WHO), the annual occurrence rate of CE in endemic areas exceeds 50 per 100,000 individuals. In certain regions, the prevalence rate reaches 5%–10%, and the infection rate in slaughtered livestock can be as high as 20%–95% [6]. The Global Burden of Disease Study 2021 reported that the global age-standardized prevalence rate of CE is 7.69 per 100,000 individuals [7]. This disease causes approximately $2 billion in annual economic losses to the livestock industry and affects nearly 1 million people worldwide, posing a significant threat to human health and public safety [8].

The liver is the primary target organ for *E. granulosus* infection. Following parasitization, protoscoleces gradually develop into expanding hydatid cysts, which mechanically compress the surrounding hepatic tissue. This process simultaneously induces inflammatory cell infiltration, fibroblast proliferation, chronic inflammatory responses, and hepatic fibrosis. These pathological changes lead to disrupted hepatocyte metabolic function and impaired liver function, ultimately resulting in irreversible liver damage and potentially organ failure [9]. Furthermore, *E. granulosus* employs immune evasion strategies to suppress the host immune response, thereby facilitating parasite survival and disease progression, which poses significant challenges for clinical treatment [10, 11].

Currently, the standard treatment plans for hepatic cystic echinococcosis (CE) include surgical intervention, percutaneous aspiration-injection-reaspiration (PAIR), pharmacotherapy, and watchful waiting [12]. However, because clinical manifestations of CE typically emerge in the advanced stages of the disease, there exists a substantial population of asymptomatic carriers, leading to difficulties in early diagnosis[13]. Although surgical resection offers the potential for radical cure, it is associated with significant trauma, a high incidence of complications, and a considerable risk of recurrence [14]. Meanwhile, the long-term first-line drug, albendazole (ABZ), presents several challenges, including substantial hepatotoxicity, low bioavailability, and the risk of drug resistance. Furthermore, the prolonged natural course of echinococcosis development and progression results in poor patient adherence to this class of medications, with overall therapeutic efficacy remaining unsatisfactory [15, 16]. Therefore, there is an urgent need to develop safer and more effective novel anti-echinococcosis drugs to provide additional therapeutic options for the management of this disease.

Harmine (HM) is a β-carboline alkaloid, also known as banisterine, that is widely distributed in plants of the genus *Peganum* (family Zygophyllaceae). HM exhibits a broad spectrum of biological activities, including antitumor, anti-echinococcal, anti-inflammatory, and immunomodulatory effects [17]. In vitro and in vivo pharmacodynamic studies have confirmed the therapeutic efficacy of HM against cystic

echinococcosis [18]. However, HM has also been found to possess significant neurotoxicity, which is mediated through the inhibition of amine neurotransmitters or direct interaction with specific receptors, thereby stimulating the central nervous system. Administration of high-dose HM can induce tremors, convulsions, paroxysmal seizures, opisthotonos, and ataxia in both animals and humans, with severe cases leading to death [19]. The substantial neurotoxicity of HM has hindered its clinical translation. To mitigate its neurotoxicity, researchers are dedicated to structural modification of HM to obtain derivatives with high efficacy and low toxicity. Our research team synthesized an HM derivative, 1-methyl-9-((3-pyridyl) methyl)-β-carboline (designated as H-2-168), through structural modification of the HM using computer-aided design(Fig. 1). Our previous studies have demonstrated that H-2-168 exhibits superior safety profiles compared to HM both in vivo and in vitro, and possesses better anti-cystic echinococcosis efficacy than the positive control drug ABZ. [18]. However, the specific molecular mechanisms by which H-2-168 exerts its effects through the modulation of metabolism and protein expression during *E. granulosus* infection have not yet been reported and warrant further investigation.

Metabolomics, as a core tool for investigating dynamic metabolic changes in organisms, enables the direct assessment of cellular or tissue biochemical status and the extent of metabolic disorders by detecting differential expression profiles of small-molecule metabolites in vivo. This approach has been widely applied in fields such as liver diseases and parasitic infections, providing an effective means for identifying potential biomarkers and key metabolic pathways [20]. Proteomics, in turn, systematically analyzes the expression profiles and regulatory networks of proteins within an organism and can be employed to screen for functional proteins associated with parasitic infections, offering important support for disease diagnosis and drug target selection [21, 22]. Following infection with *E. granulosus*, the host liver exhibits numerous differentially expressed proteins involved in processes including immune evasion, inflammatory responses, and metabolism regulation [23]. Furthermore, the combined application of proteomics and metabolomics enables an integrated cross-level analysis of the protein–metabolite interaction, thereby facilitating a more comprehensive understanding of the molecular mechanisms underlying disease pathogenesis and interventional regulation [24].

In this study, mice infected with *E. granulosus* were treated with H-2-168. Metabolomic and proteomic analyses of liver tissues were conducted using liquid chromatography-tandem mass spectrometry (LC-MS/MS) to identify differentially expressed metabolites (DEMs) and proteins following H-2-168 intervention. By integrating KEGG pathway enrichment analysis with the multi-omics data, the key molecular pathways and regulatory networks underlying the effects of H-2-168 on *E. granulosus* infection were identified. This approach revealed the intervention mechanism of H-2-168 and provides novel experimental evidence and potential therapeutic targets for the clinical management of cystic echinococcosis.

Methods

Materials

HM and H-2-168(purity > 98%) were supplied by Xinjiang Huashidan Pharmaceutical Co., Ltd (Xinjiang, China).

Animals

Female BALB/c mice, aged 6–8 weeks and weighing 20 ± 2 g, were selected for this study. All mice were housed under specific pathogen-free (SPF) barrier conditions at the Animal Experiment Center of Xinjiang Medical University. The environment was maintained at a constant temperature and humidity, with a 12-hour light/12-hour dark cycle. The animals had ad libitum access to food and water. Prior to the experiment, the mice were fasted overnight with water deprivation.

Protoscoleces (PSCs) collection and culture

Following standard aseptic procedures, sheep liver tissues infected with *E. granulosus* were collected from local slaughterhouse. After gently wiping the surface contaminants from the liver tissues using sterile dry gauze, the hydatid cyst fluid and cyst wall tissues were aseptically collected within a laminar flow hood. The protoscoleces (PSCs) were isolated via tissue homogenization, repeated washing, and filtration steps. The purified protoscoleces were then digested with 1% pepsin (pH 2.0–3.0) at 37°C for 30 min [24]. The viability of protoscoleces was assessed using the eosin exclusion test, and only those with a viability rate greater than 95% were selected for subsequent in vivo animal experiments.

Establishment of E. granulosus infection mouse model

BALB/c mice were categorized into three groups (n = 6) based on the intervention method: control group, model group, and H-2-168-treated group. In the model group and the H-2-168 group, mice were inoculated via the hepatic portal vein with 0.2 mL of normal saline suspension containing 2,000 PSCs (viability ≥ 95%) to establish a mouse model of CE. Mice in the control group received an equivalent volume of normal saline injected into the hepatic portal vein[24]. After three months of housing in SPF environment, the successful establishment of the model in both the model group and the H-2-168 group was confirmed via B-mode ultrasound examination. Subsequently, mice in the H-2-168 group received a daily oral dose of 100 mg/kg for 30 consecutive days. Mice in the control group and the model group were administered an equivalent volume of normal saline via gavage, following the same schedule as the intervention group. The dosage of H-2-168 was determined based on our previous study in rats, where the 100 mg/kg dose was identified as an effective and safe oral dose level[25]. This dosage ensures adequate in vivo drug exposure, meeting the requirements for detecting the drug intervention effect in subsequent omics analyses.

Following the intervention period, mice were anesthetized with inhaled isoflurane. After achieving deep anesthesia, the mice were euthanized by cervical dislocation. Prior to euthanasia, blood samples were collected via orbital bleeding. Subsequently, the mice were dissected, and liver samples were collected and stored appropriately for subsequent analyses.

Metabolomics Analysis

Liver tissue samples from the model group and the H-2-168 group were selected for metabolomics analysis, with three mice randomly chosen from each group. A 100 mg sample of mouse liver tissue was placed in a centrifuge tube containing a mixture of 75% methanol and 25% deionized water, along with steel beads, and homogenized at room temperature for 30 minutes. Following homogenization, the mixture was centrifuged, and the supernatant was collected and concentrated [24]. The concentrated sample was then reconstituted in a 50% acetonitrile solution and analyzed using a Vanquish liquid chromatography system (Thermo Fisher Scientific, MA, USA) coupled with an Orbitrap Exploris 120 mass spectrometer (Thermo Fisher Scientific, MA, USA) for liquid chromatography-mass spectrometry (LC-MS) detection [24]. The raw data obtained were compared against the Human Metabolome Database (HMDB), the MassBank database, and the Kyoto Encyclopedia of Genes and Genomes (KEGG) for metabolite identification. Differentially enriched metabolites were identified using the criteria of $|\log_2 \text{FoldChange}| \geq 1$ and $P < 0.05$ [26, 27].

Proteomic Analysis

Concurrently with the aforementioned metabolomic analysis, proteomic analysis was conducted. Liver samples were collected from the model group and the H-2-168 group, with liver tissues from three randomly selected mice per group used for this analysis. Following hepatic protein extraction, the protein concentration was determined using the BCA assay, and extraction efficiency was evaluated via SDS-PAGE electrophoresis. Protein enzymatic digestion and desalting were performed using the MagicMomics Microproteomics Sample Preparation Kit (QLBio, Beijing, China), and the samples were lyophilized for subsequent use. The digested and desalted samples were analyzed by liquid chromatography-tandem mass spectrometry (LC-MS/MS) using an Orbitrap Exploris™ 480 mass spectrometer (Thermo Fisher Scientific, Massachusetts, USA) [24]. After data processing with Spectronaunt software, differentially expressed proteins were identified based on the criteria of $|\log_2 FC| \geq 1$ and FDR < 0.05 [28, 29]. Functional annotation of these differentially expressed proteins was performed using Gene Ontology (GO) enrichment analysis and Kyoto Encyclopedia of Genes and Genomes (KEGG) pathway analysis to investigate their biological functions and regulatory mechanisms [29, 30].

Integrated Metabolomics and Proteomics Analysis

Multi-omics integrative analysis was performed on differential metabolites and differential proteins. Based on Pearson correlation calculation, with a threshold of correlation coefficient $|r| > 0.8$ and $P < 0.05$, a correlation heatmap and an interaction network map were constructed to systematically present the correlation patterns among molecules [31]. The expression trends of differential proteins and differential metabolites were analyzed using a nine-quadrant diagram to screen for key molecular pairs with potential regulatory relationships. Joint enrichment analysis of KEGG pathways was conducted for the

differential molecules from the two omics datasets, and commonly enriched pathways were identified using Venn diagrams, bubble charts, and pathway networks. Canonical correlation analysis (CCA) and orthogonal partial least squares analysis (O2PLS) were employed to dissect the overall correlation characteristics. Furthermore, enzyme-substrate association analysis was performed to elucidate the regulatory relationships between proteins and metabolites within metabolic pathways, thereby untangling the underlying biological regulatory mechanisms from a systems-level perspective [32, 33].

Statistical Analysis

All statistical analyses were performed using SPSS software (version 26.0, IBM, USA), and experimental figures were generated using GraphPad Prism (version 9.0, GraphPad Software, USA). Continuous data are presented as mean ± standard deviation ($\bar{x}$ ± s), while categorical data are expressed as frequencies (n) or percentages (%). All experiments were independently repeated at least three times. Statistical significance of differences between groups was evaluated using Student's t-test or one-way analysis of variance (one-way ANOVA). Correlations between variables were analyzed using Spearman's rank correlation coefficient. A P-value of less than 0.05 was considered statistically significant.

Results

Analysis of Differentially Expressed Metabolites between the H-2-168 and Model Groups

Untargeted metabolomics profiling using LC-MS/MS was performed on liver tissue samples from the model group and the H-2-168 group. Compared with the model group, a total of 440 metabolites were identified in the H-2-168 group, among which 87 exhibited differential expression, including 54 upregulated and 33 downregulated metabolites (Fig. 2A). A correlation heatmap of the differentially expressed metabolites(DEMs) (Fig. 2B) further supported these findings, with the color intensity of the bidirectional hierarchical clustering tree indicating the strength of correlations among metabolites. A differential molecular heatmap was employed to visually illustrate the differences in metabolite abundance between the groups (Fig. 2C). The volcano plot (Fig. 2D) and the scatter plot of metabolite mass-to-charge ratios versus P-values (Fig. 2E) revealed that, relative to the model group, metabolites such as L-2-amino-6-oxoheptanedioic acid, α-linolenic acid, and L-aspartic acid were significantly upregulated in the H-2-168 group, while metabolites including creatinine, methyldopa, and all-trans retinoic acid were significantly downregulated.

Subsequently, KEGG pathway enrichment analysis was conducted on the DEMs. The results indicated that the key metabolic pathways exhibiting significant differences between the two groups primarily included linoleic acid metabolism, arginine biosynthesis, and peroxisome proliferator-activated receptor (PPAR) signaling pathway (Figs. 3A, 3C). The highly significantly enriched metabolic pathways are summarized in Table 1. A statistical chart of the number of differentially enriched metabolites in these pathways (Fig. 3B) showed that a higher number of upregulated metabolites were involved in D-amino

acid metabolism and ABC transporters, whereas a greater number of downregulated metabolites were associated with linoleic acid metabolism and the serotonergic synapse pathway. A metabolite–KEGG pathway association network diagram demonstrated that dozens of metabolites involved in the aforementioned core metabolic pathways were significantly either upregulated or downregulated (Fig. 3D).

Table 1
Metabolic pathways with highly significant enrichment differences

Number	Differential pathways	Hits	*P* value	FDR
1	Linoleic acid metabolism	5/28	0.00051	0.05047
2	Central carbon metabolism in cancer	5/37	0.00190	0.07038
3	Arginine biosynthesis	4/23	0.00213	0.07038
4	Alanine, aspartate and glutamate metabolism	4/28	0.00449	0.09320
5	PPAR signaling pathway	2/5	0.00572	0.09320
6	D-Amino acid metabolism	6/69	0.00652	0.09320
7	Phenylalanine metabolism	5/49	0.00659	0.09320
8	Neuroactive ligand-receptor interaction	5/53	0.00918	0.11364
9	Glutathione metabolism	4/38	0.01343	0.14772
10	ABC transporters	8/139	0.02003	0.19834
11	Protein digestion and absorption	4/47	0.02746	0.24715
12	Biosynthesis of unsaturated fatty acids	5/74	0.03451	0.28469
13	beta-Alanine metabolism	3/32	0.04292	0.32682
14	Intestinal immune network for IgA production	1/2	0.04870	0.34441
15	Vitamin digestion and absorption	3/39	0.07001	0.39694
16	Efferocytosis	2/18	0.07121	0.39694
17	Renal cell carcinoma	1/3	0.07217	0.39694
18	Small cell lung cancer	1/3	0.07217	0.39694
19	Cysteine and methionine metabolism	4/67	0.08179	0.40404
20	Serotonergic synapse	3/42	0.08349	0.40404

Analysis of Differentially Expressed Proteins Between the H-2-168 and Model Groups

Quantitative analysis of liver tissues from the model group and the H-2-168 group was performed using label-free quantitative proteomics based on LC-MS/MS. A total of 238 differentially expressed proteins were identified in the H-2-168 group, of which 113 were significantly upregulated and 125 were downregulated (Fig. 4A, B). The top 10 differentially expressed proteins ranked by fold change are listed in Table 2.

Table 2
Differentially Upregulated and Downregulated Proteins

Number	Gene Name	Expression type	*P* Value	FC
1	Pno1	up	0.00493	7.69195
2	Ighv5-17	up	0.00481	6.56925
3	Rd3	up	0.00292	5.19705
4	Mlh1	up	0.03707	4.03402
5	Sypl1	up	0.02211	3.93141
6	Flcn	up	0.00369	3.74193
7	Tmem168	up	0.01847	3.71009
8	Mtf2	up	0.01848	3.63100
9	Tspan31	up	0.01583	3.46105
10	Igkv13-84	up	0.00148	3.45600
11	Pcbp1	down	0.01495	0.66307
12	Ndufaf7	down	0.03148	0.65940
13	Cobll1	down	0.00386	0.65793
14	Pcna	down	0.01575	0.65601
15	Nbn	down	0.01825	0.65553
16	Klhl9	down	0.01339	0.64978
17	Txndc9	down	0.03014	0.64336
18	Casp9	down	0.00261	0.63853
19	Opa3	down	0.00450	0.63785
20	Steap3	down	0.00494	0.63357

Gene Ontology (GO) cellular component enrichment analysis (Fig. 4C) revealed that the mitochondrion was the most significantly enriched cellular component, with an enrichment ratio of approximately 0.2. In addition, several mitochondrial substructures and functional complexes were also significantly enriched,

including the mitochondrial inner membrane, mitochondrial matrix/mitochondrial nucleoid, and the mitochondrial fatty acid beta-oxidation multienzyme complex. Furthermore, the peroxisome and its subcompartments (peroxisomal matrix, peroxisomal membrane) were also significantly enriched. Biological process enrichment analysis (Fig. 4D) indicated that the differentially expressed proteins between the model and treatment groups were primarily enriched in pathways related to the inflammation-lipid metabolism axis, immune regulation, and cellular metabolism. Among these, significantly enriched processes included cellular response to nutrients, icosanoid biosynthetic process, the inflammatory response, and its positive regulation. Molecular function enrichment analysis (Fig. 4E) showed that flavin adenine dinucleotide binding was the most significantly enriched molecular function. The largest numbers of differentially expressed proteins were associated with oxidoreductase activity, iron ion binding, and heme binding. Additionally, multiple oxidoreductase- and metabolism-related enzyme activities were significantly enriched. KEGG pathway enrichment analysis showed that the differentially expressed proteins were significantly associated with retinol metabolism, peroxisomal pathways, inflammatory regulation of the TRP pathway, PPAR and mitogen-activated protein kinase (MAPK) signaling pathways (Fig. 4F).

Integrated proteomics and metabolomics analysis following H-2-168 intervention

Integrated omics analysis showed that *E. granulosus* infection disrupted host metabolic and protein regulatory networks. Pathway enrichment analysis (Fig. 5A) identified tryptophan metabolism, sphingolipid metabolism/sphingolipid signaling pathway, and ferroptosis as core pathways significantly altered at both the proteomic and metabolomic levels. The KEGG interaction network (Fig. 5B) identified 8 signaling pathways, 9 key proteins, and 18 key metabolites, showing interconnections between core pathways and those related to immunity and energy metabolism. The correlation network (Fig. 5D) included 17 metabolites and 35 proteins, revealing complex positive and negative regulatory interactions. Nine-quadrant association analysis (Fig. 5E) revealed multiple regulatory patterns, including co-directional changes, inverse changes, and omics-specific changes, indicating multi-layer and differential regulation of molecular expression under infection. A clustered heatmap of the top 50 proteins and metabolites ranked by lowest *P* values (Fig. 5F) clearly distinguished the model group from the H-2-168 group, showing significant expression clustering. A Venn diagram (Fig. 5C) visualizes overlapping molecular datasets.

Discussion

Treatment of echinococcosis remains clinically challenging, necessitating novel therapeutic strategies. Thus, there is an urgent need to develop new anti-echinococcal drugs and elucidate their mechanisms of action. In this study, we integrated metabolomics and quantitative proteomics to investigate the regulatory effects of the harmine derivative H-2-168 on liver metabolites and proteins in *E. granulosus*-infected mice. Our aim was to elucidate the molecular mechanism underlying its

anti-echinococcal activity from a host-parasite interaction perspective, thereby providing a multi-omics basis for further evaluation of H-2-168 as a potential therapeutic agent.

Integrated multi-omics analysis showed that H-2-168 intervention primarily altered linoleic acid metabolism, amino acid metabolism, the tricarboxylic acid (TCA) cycle, and the PPAR signaling pathway. Thus, H-2-168 not only affects parasite energy synthesis and metabolic processes but also modulates host immune and lipid metabolic networks.

Previous studies have demonstrated that *E. granulosus* lacks the complete enzyme system for de novo synthesis of polyunsaturated fatty acids and relies on host-derived essential fatty acids for growth and development [34]. Genomic and transcriptomic analyses have identified the absence of key genes in the fatty acid synthesis pathway, compelling the parasite to acquire lipids from the host [35–37]. Disruption of this pathway impairs parasite membrane synthesis and energy supply. In the present study, significant enrichment of linoleic acid metabolism at both omics levels confirms that H-2-168 acts by blocking the supply of essential fatty acids to the parasite, consistent with previous reports.

Significant differences were also observed in amino acid metabolism, including alanine, aspartate, and glutamate metabolism. H-2-168 also significantly downregulated key TCA cycle intermediates, such as fumarate, indicating that it inhibits the energy production process coupled with glycolysis and the TCA cycle in the parasite. Disruption of metabolic energy is a well-established mechanism for inhibiting the survival, proliferation, and development of Echinococcus protoscoleces [38]. The enrichment of mitochondria-related components in the proteomics analysis further confirms disruption of parasite energy metabolism, consistent with the dependence of *E. granulosus* protoscoleces on mitochondrial energy supply.

Studies have shown that during Echinococcus infection, the parasite mediates host immune evasion through arginine consumption, and imbalance of arginine metabolism is a key pathway for this evasion [39]. The significant alterations in arginine metabolism-related pathways observed in this study suggest that H-2-168 enhances host innate immune clearance of Echinococcus by regulating arginine metabolism and nitric oxide production.

Furthermore, the marked alterations in glutathione metabolism and redox-related metabolites suggest that H-2-168 may exert its anti-cystic echinococcosis effects by influencing oxidative stress. Decreased glutathione levels are closely associated with oxidative stress and liver injury [40, 41]. Given that Echinococcus is highly sensitive to oxidative stress, disrupting its antioxidant system is a crucial strategy for anti-echinococcal drug development [42, 43]. The differential expression of oxidoreductase activity and mitochondria-related proteins in our proteomics analysis further supports this mechanism.

In addition to redox regulation, H-2-168 modulated lipid-related signaling pathways. The PPAR signaling pathway was significantly enriched in both omics datasets, suggesting that H-2-168 improves the infection microenvironment by regulating host lipid metabolism and inflammatory responses. This

pathway has been shown to participate in host defense and inhibition of parasite growth in various parasitic infection models [44–46], supporting our findings across species.

Complementing the metabolomics findings, our proteomic analysis also provided further mechanistic insights. GO functional analysis revealed enrichment of mitochondrial and endoplasmic reticulum components, as well as pathways related to immune regulation and stress response. This enrichment supports the conclusion that H-2-168 disrupts parasite energy metabolism and inhibits parasite immune evasion. Enrichment of cytochrome P450 binding activity suggests interference with the parasite's metabolic enzyme system. This protein family plays a critical role in parasite drug metabolism, and altered expression of CYPs has been associated with drug resistance in various parasites [47, 48], suggesting that H-2-168 may have the potential to modulate drug resistance.

Integrated analysis of the two omics datasets revealed that H-2-168 regulates both metabolic networks and protein functions in a coordinated manner. Furthermore, a clustered heatmap demonstrated consistency of the intervention effects across the two omics datasets.

Several limitations should be considered. First, the use of whole liver tissue homogenates did not allow discrimination between host-derived and parasite-derived signals. Thus, the relative contribution of each to the observed multi-omics changes remains to be disentangled. Second, functional validation of the identified targets (e.g., through pharmacological inhibition or enzyme activity assays) was not performed in this study. Finally, the omics data were collected at a single time point after H-2-168 intervention, precluding assessment of the temporal dynamics of the host-parasite metabolic crosstalk. Nevertheless, these limitations do not diminish the main conclusion that H-2-168 exerts multi-level regulatory effects on host-parasite metabolic and protein networks, providing a multi-omics foundation for further evaluating H-2-168 as a potential anti-cystic echinococcosis therapeutic agent.

Conclusions

In *E. granulosus*-infected mice, H-2-168 exerts anti-parasitic effects through multiple metabolic and immune pathways. H-2-168 disrupts parasite metabolic homeostasis by interfering with linoleic acid metabolism, amino acid metabolism, and the TCA cycle. H-2-168 also reduces parasite immune evasion and improves the host infection microenvironment by regulating oxidative stress, arginine metabolism, and the PPAR signaling pathway, thereby inhibiting parasite survival and development. This study identified key differential metabolites and proteins associated with the anti-echinococcal effects of H-2-168. These findings provide a basis for future target validation and the development of candidate drugs against cystic echinococcosis.

Abbreviations

CE
Cystic echinococcosis
E. granulosus

Echinococcus granulosus
WHO
World Health Organization
ABZ
albendazole
SPF
specific pathogen-free
PSCs
protoscoleces
LC-MS/MS
liquid chromatography-tandem mass spectrometry
KEGG
Kyoto Encyclopedia of Genes and Genomes
GO
Gene Ontology
DEMs
differentially expressed metabolites
PPAR
peroxisome proliferator-activated receptor
MAPK
mitogen-activated protein kinase.

Declarations

Acknowledgements

We thank BioGDP (www.biogdp.com) for providing the illustration platform and icons used in the graphical abstract.

Funding

This work was supported by “Tianshan Talent” Program for Training High-level Talents in Medicine and Healthcare [TSYC202401B058], Xinjiang Uygur Autonomous Region Natural Science Foundation [2023D01D16], China International Medical Exchange Foundation-Clinical Pharmacy Branch of Chinese Medical Association 2023 Clinical Pharmacy Research Fund [Z-2021-46-2101-2023], Scientific Research Fund of Xinjiang Uygur Autonomous Region Pharmaceutical Association [YXH202406].

Availability of data and materials

The datasets supporting the conclusions of this article are included within the article and its additional files.

Authors' contributions

YXYM conducted the experiments and drafted the manuscript. QWX and YJH analyzed the metabolomic data, JXL and HYX analyzed the proteomics data, HJG and TL designed the study and critically revised the manuscript. All authors read and approved the final manuscript.

Ethics approval and consent to participate

All mice experimental protocols were reviewed and approved by the Animal Ethics Committee of the First Affiliated Hospital of Xinjiang Medical University (Approval number: IACUC-20230321014). All operational procedures were performed in strict accordance with the ethical standards and guidelines for the care and use of laboratory animals.

Consent for publication

Not applicable.

Competing interests

The authors declare that they have no competing interests.

Author details

[1]College of Pharmacy, Xinjiang Medical University, Urumqi, China

[2]State Key Laboratory of Pathogenesis, Prevention and Treatment of High Incidence Diseases in Central Asia, Xinjiang Medical University, Urumqi, China

[3]Department of Pharmacy, The First Affiliated Hospital of Xinjiang Medical University, Urumqi, China

[4]Department of Pharmacy, People's Hospital of Bayingolin Mongolian Autonomous Prefecture, Xinjiang Uygur Autonomous Region, Korla, China

References

1. Eckert J, Deplazes P. Biological, epidemiological, and clinical aspects of echinococcosis, a zoonosis of increasing concern. Clin Microbiol Rev. 2004;17:107–35. https://doi.org/10.1128/CMR.17.1.107-135.2004
2. Wen H, Vuitton L, Tuxun T, Li J, Vuitton DA, Zhang W, et al. Echinococcosis: Advances in the 21st century. Clin Microbiol Rev. American Society for Microbiology; 2019;32:e00075-18. https://doi.org/10.1128/cmr.00075-18
3. Wang Z, Pu N, Zhao W, Chen X, Zhang Y, Sun Y, et al. RNA sequencing reveals dynamic expression of genes related to innate immune responses in canine small intestinal epithelial cells induced by

echinococcus granulosus protoscoleces. Front Vet Sci [Internet]. Frontiers; 2024 [cited 2026 Apr 16];11. https://doi.org/10.3389/fvets.2024.1503995

4. Bosco A, Alves LC, Cociancic P, Amadesi A, Pepe P, Morgoglione ME, et al. Epidemiology and spatial distribution of echinococcus granulosus in sheep and goats slaughtered in a hyperendemic european mediterranean area. Parasites Vectors. 2021;14:421. https://doi.org/10.1186/s13071-021-04934-9
5. Shahla HS, Zahra S. Echinococcus granulosus, a parasite producing hydatid cyst: a review. Arch Razi Inst. 2025;80:543–8. https://doi.org/10.32592/ARI.2025.80.3.543
6. Hogea M-O, Ciomaga B-F, Muntean M-M, Muntean A-A, Popa MI, Popa GL. Cystic echinococcosis in the early 2020s: a review. Trop Med Infect Dis. 2024;9:36. https://doi.org/10.3390/tropicalmed9020036
7. Wang Y, Zhang R, Zhang D, Liang Y, Xu C, Zhang C. Global burden of cystic echinococcosis: a 32-year analysis of 204 countries with 2036 projections. BMC Public Health. 2025;25:3213. https://doi.org/10.1186/s12889-025-24502-5
8. Li B, Quzhen G, Xue C-Z, Han S, Chen W-Q, Yan X-L, et al. Epidemiological survey of echinococcosis in tibet autonomous region of China. Infect Dis Poverty. 2019;8:29. https://doi.org/10.1186/s40249-019-0537-5
9. Zhai S, Yang Y, Zhou Y, Lai Q, Li K, Liu S, et al. Echinococcus granulosus-induced liver damage through ferroptosis in rat model. Cells. Multidisciplinary Digital Publishing Institute; 2025;14:328. https://doi.org/10.3390/cells14050328
10. He R, Yan R, Shi Y, Aierken A, Zhang X, Wen H, et al. Multi-omics approaches reveal the mechanisms underlying the interaction between cyst fluid of echinococcus granulosus and host immune cells. Front Immunol [Internet]. Frontiers; 2025 [cited 2026 Apr 20];16. https://doi.org/10.3389/fimmu.2025.1598028
11. Wang S, Jiang D, Huang F, Qian Y, Qi M, Li H, et al. Therapeutic effect of echinococcus granulosus cyst fluid on bacterial sepsis in mice. Parasites Vectors. 2023;16:450. https://doi.org/10.1186/s13071-023-06021-7
12. Ferreira AI, Xavier S, Lopes P, Marinho C, Cotter J. Echinococcosis: a challenging treatment. GE - Port J Gastroenterol. 2026;33:384–6. https://doi.org/10.1159/000550702
13. Zhu M, Du X, Xu H, Yang S, Wang C, Zhu Y, et al. Metabolic profiling of liver and faeces in mice infected with echinococcosis. Parasites Vectors. BioMed Central; 2021;14:324. https://doi.org/10.1186/s13071-021-04807-1
14. Paramita AAKY, Wibawa IDN. Multimodal treatment of cystic echinococcosis. Indones J Gastroenterol Hepatol Dig Endosc. 2023;24:72–82. https://doi.org/10.24871/241202372-82
15. Qin M, Yang G, Yan J, Wang L, Feng Y, Wang D, et al. Assessment of compliance and therapeutic efficacy of albendazole treatment in chinese patients with echinococcosis. Infect Dis Poverty. 2024;13:98. https://doi.org/10.1186/s40249-024-01268-3

16. Siles-Lucas M, Casulli A, Cirilli R, Carmena D. Progress in the pharmacological treatment of human cystic and alveolar echinococcosis: compounds and therapeutic targets. PLoS NeglTrop Dis. Public Library of Science; 2018;12:e0006422. https://doi.org/10.1371/journal.pntd.0006422
17. Hu Y, Yu X, Yang L, Xue G, Wei Q, Han Z, et al. Research progress on the antitumor effects of harmine. Front Oncol. 2024;14:1382142. https://doi.org/10.3389/fonc.2024.1382142
18. Chen B, Yan M, Gao H, Ma Q, Li L, Lü G, et al. In vitro and in vivo efficacies of novel harmine derivatives in the treatment of cystic echinococcosis. Drug Des Dev Ther. Dove Press; 2023;17:2441–54. https://doi.org/10.2147/DDDT.S419002
19. Lv Y, Liang H, Li J, Li X, Tang X, Gao S, et al. Central inhibition prevents the in vivo acute toxicity of harmine in mice. J Toxicol Sci. 2021;46:289–301. https://doi.org/10.2131/jts.46.289
20. Gao H, Xu Q, Zhu J, Kuerban K, Chen B, Zhao J, et al. Efficacy and mechanism of action of harmine derivative H-2-104 against echinococcus granulosus infection in mice. BMC Vet Res. 2025;21:174. https://doi.org/10.1186/s12917-025-04642-x
21. Dąbrowska J, Sroka J. A multi-omics perspective on tritrichomonas foetus: from genomics to future directions. Int J Mol Sci. 2025;26:8343. https://doi.org/10.3390/ijms26178343
22. Shanley HT, Wang T, Taki AC, Byrne JJ, Chang BCH, Sleebs BE, et al. Advances in anthelmintic target identification. Int J Mol Sci. 2025;26:3738. https://doi.org/10.3390/ijms26083738
23. Jiang N, Chen Y, Li T, Sun Y, Su Y, Wang Y, et al. Proteomic analysis of mouse liver lesions at all three stages of echinococcus granulosus infection. PLoS NeglTrop Dis. Public Library of Science; 2024;18:e0012659. https://doi.org/10.1371/journal.pntd.0012659
24. Zhu J, Zhou T, Chen G, Gao H, Chen X, Tuohetali A, et al. GHSR gene knockout alleviates the liver pathological response in echinococcus granulosus infection by reducing parasite survival. Vet Res. 2025;56:55. https://doi.org/10.1186/s13567-025-01478-z
25. Bahatijiang M, Xu N, Hu X, Liu W, Lei J, Zhang S, et al. Simultaneous quantification of a novel β-carboline alkaloid derivative and its three metabolites in rat plasma by UHPLC-MS/MS and its application to a pharmacokinetic study. J Sep Sci. 2025;48:e70282. https://doi.org/10.1002/jssc.70282
26. He Q, Ye B, Li H, Pan Y, Du Y, Yang K. Analysis of potential biomarkers for diabetic kidney disease and non-diabetic kidney disease based on urinary metabolomics analysis. BMC Nephrol. 2025;26:612. https://doi.org/10.1186/s12882-025-04544-y
27. Wang J, Zhang Q, Chen J, Zhou J, Li J, Wei Y, et al. Combined transcriptome and metabolome analysis of a new species of microalgae from the Tibetan Plateau and its response to sewage treatment. Water. 2022;14:3391. https://doi.org/10.3390/w14213391
28. Biełło KA, Die JV, Amil F, Fuentes-Almagro C, Pérez-Rodríguez J, Olaya-Abril A. Reproducibility crossroads: impact of statistical choices on proteomics functional enrichment. Int J Mol Sci. 2025;26:9232. https://doi.org/10.3390/ijms26189232
29. Zhang M, Zhao Y, Du J, Cui J, Huang M, Wang J, et al. Integration of multi-omics data and phenotyping provides insights into purple leaf sheaths color in millet seedling stage. BMC Plant Biol.

2025;25:1645. https://doi.org/10.1186/s12870-025-07652-x

30. Tang C, Fan Y, Wang T, Wang J, Xiao M, He M, et al. Integrated amino acid profiling and 4D-DIA proteomics reveal protein quality divergence and metabolic adaptation in cordyceps species. J Fungi. 2025;11:365. https://doi.org/10.3390/jof11050365
31. Yang B, Zhang Z, Liu Y, Gong Z, Wu G. Integrated proteomics and metabolomics analysis revealed that macrophage-related signals may be potential biomarkers for oral squamous cell carcinoma. Sci Rep. Nature Publishing Group; 2025;16:2217. https://doi.org/10.1038/s41598-025-31899-x
32. Wang Q, Jiang Q, Liu J, Zhang P, Li L, Li H, et al. Integrated transcriptomic and metabolomic analysis reveals key genes and core metabolic pathways involved in phosphorus stress response in quinoa flower spikes. BMC Plant Biol. 2025;25:1588. https://doi.org/10.1186/s12870-025-07649-6
33. Yu S, Huang Y, Wu C, Fu W, Liang H, Chen C, et al. Integrated multi-omic characterization of the detachment process of adherent vero cells with animal-based and animal-origin-free enzymes. Cells. 2022;11:3396. https://doi.org/10.3390/cells11213396
34. Silva-Álvarez V, Franchini GR, Pórfido JL, Kennedy MW, Ferreira AM, Córsico B. Lipid-free antigen B subunits from echinococcus granulosus: Oligomerization, ligand binding, and membrane interaction properties. PLoS NeglTrop Dis. Public Library of Science; 2015;9:e0003552. https://doi.org/10.1371/journal.pntd.0003552
35. Debarba JA, Sehabiague MPC, Monteiro KM, Gerber AL, Vasconcelos ATR, Ferreira HB, et al. Transcriptomic analysis of the early strobilar development of echinococcus granulosus. Pathogens. 2020;9:465. https://doi.org/10.3390/pathogens9060465
36. Obal G, Ramos AL, Silva V, Lima A, Batthyany C, Bessio MI, et al. Characterisation of the native lipid moiety of echinococcus granulosus antigen B. PLoS NeglTrop Dis. Public Library of Science; 2012;6:e1642. https://doi.org/10.1371/journal.pntd.0001642
37. Zheng H, Zhang W, Zhang L, Zhang Z, Li J, Lu G, et al. The genome of the hydatid tapeworm echinococcus granulosus. Nat Genet. Nature Publishing Group; 2013;45:1168–75. https://doi.org/10.1038/ng.2757
38. Chaudhry S, Zurbriggen R, Preza M, Kämpfer T, Kaethner M, Memedovski R, et al. Dual inhibition of the echinococcus multilocularis energy metabolism. Front Vet Sci [Internet]. Frontiers; 2022 [cited 2026 Apr 22];9. https://doi.org/10.3389/fvets.2022.981664
39. Cao S, Gong W, Zhang X, Xu M, Wang Y, Xu Y, et al. Arginase promotes immune evasion of echinococcus granulosus in mice. Parasites Vectors. 2020;13:49. https://doi.org/10.1186/s13071-020-3919-4
40. Aimaier D, Bai W, Zhang Y, Li X, Ma C, Gu J, et al. Susceptibility factor TNF-α synergizes with polygonum multiflorum to drive idiosyncratic liver injury in mice by disrupting gut microbiota composition and hepatic metabolite homeostasis. J Inflammation Res. 2025;18:9477–94. https://doi.org/10.2147/JIR.S528667
41. Keller GA. Decreased hepatic glutathione levels in septic shock: predisposition of hepatocytes to oxidative stress: an experimental approach. Arch Surg. 1985;120:941.

https://doi.org/10.1001/archsurg.1985.01390320065013

42. Wang H, Li J, Zhang C, Guo B, Wei Q, Li L, et al. Echinococcus granulosus sensu stricto: silencing of thioredoxin peroxidase impairs the differentiation of protoscoleces into metacestodes. Parasite. EDP Sciences; 2018;25:57. https://doi.org/10.1051/parasite/2018055
43. Zhao Y, Gui W, Zhang Y, Mo G, Li D, Chong S. Inhibitory effect of ionizing radiation on echinococcus granulosus hydatid cyst. Diseases. Basel, Switzerland; 2019;7:23. https://doi.org/10.3390/diseases7010023
44. Chan MM, Evans KW, Moore AR, Fong D. Peroxisome proliferator-activated receptor (PPAR): balance for survival in parasitic infections. J Biomed Biotechnol. 2010;2010:828951. https://doi.org/10.1155/2010/828951
45. Chan MM, Fong D. The interplay of PPARs with parasites and related intracellular pathogens. PPAR Res. 2012;2012:624845. https://doi.org/10.1155/2012/624845
46. Gallardo-Soler A, Gómez-Nieto C, Campo ML, Marathe C, Tontonoz P, Castrillo A, et al. Arginase I induction by modified lipoproteins in macrophages: a peroxisome proliferator-activated receptor-gamma/delta-mediated effect that links lipid metabolism and immunity. Mol Endocrinol. Baltimore, Md.; 2008;22:1394–402. https://doi.org/10.1210/me.2007-0525
47. Dube F, Hinas A, Roy S, Martin F, Åbrink M, Svärd S, et al. Ivermectin-induced gene expression changes in adult parascaris univalens and caenorhabditis elegans: a comparative approach to study anthelminthic metabolism and resistance in vitro. Parasites Vectors. 2022;15:158. https://doi.org/10.1186/s13071-022-05260-4
48. Yilmaz E, Ramünke S, Demeler J, Krücken J. Comparison of constitutive and thiabendazole-induced expression of five cytochrome P450 genes in fourth-stage larvae of *haemonchus contortus* isolates with different drug susceptibility identifies one gene with high constitutive expression in a multi-resistant isolate. Int J Parasitol: Drugs Drug Resist. 2017;7:362–9. https://doi.org/10.1016/j.ijpddr.2017.10.001

Figures

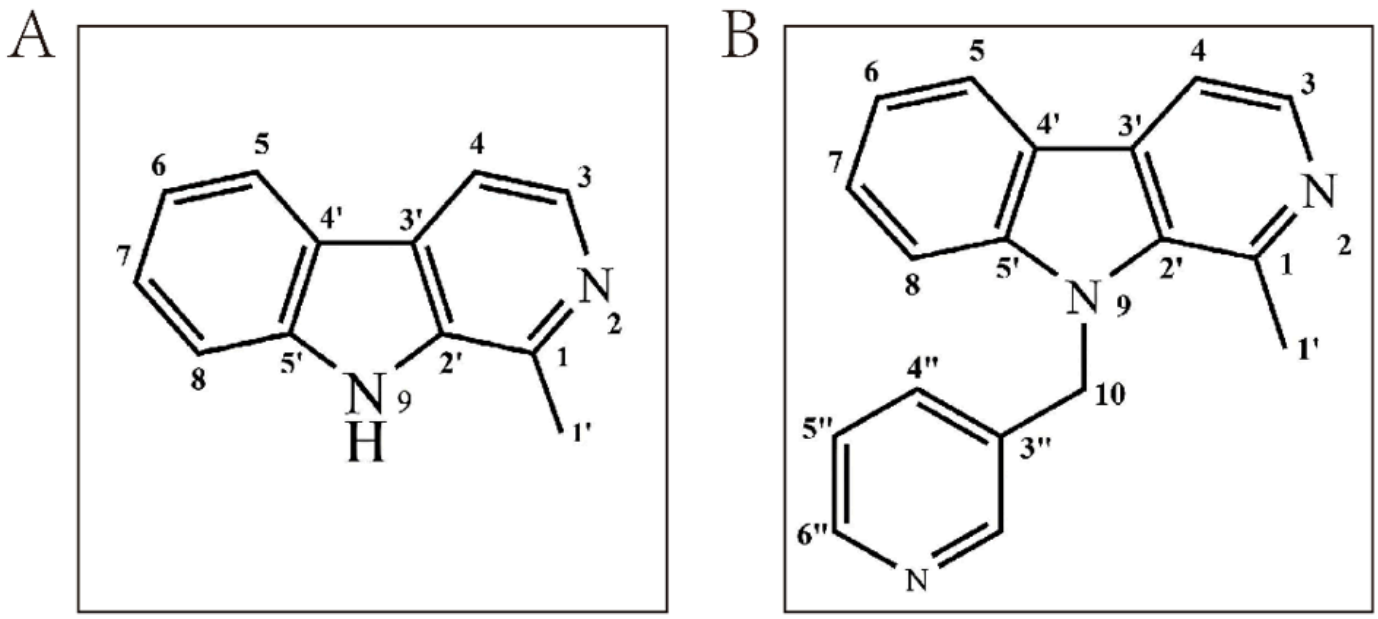


Figure 1

Chemical structures of harmine (A) and harmine derivative H-2-168 (B)

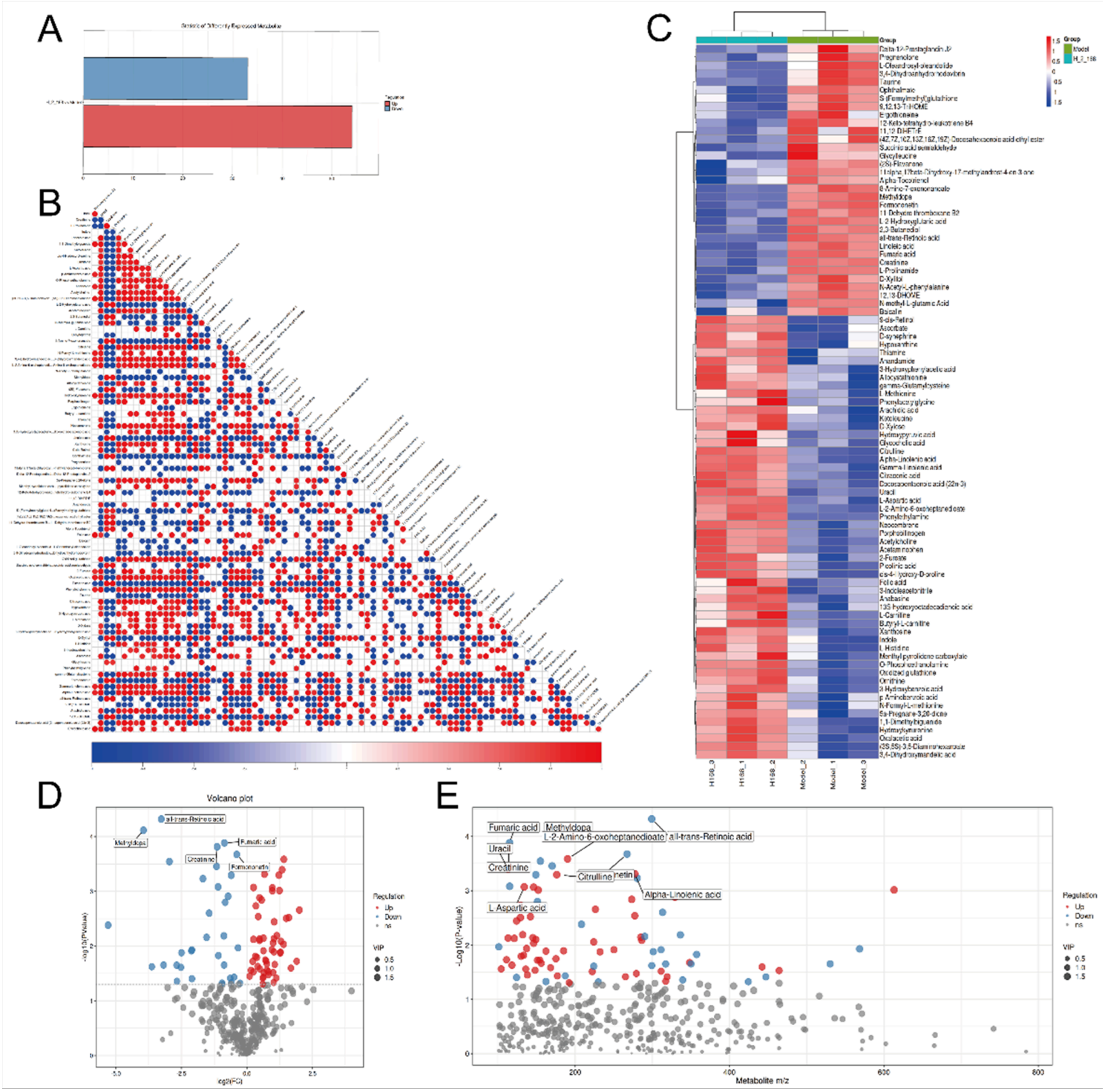


Figure 2

Screening and global characterization of differentially expressed metabolites (DEMs). **A** Differential statistics of metabolites. Bar chart showing the numbers of significantly upregulated (red) and downregulated (blue) metabolites in the H-2-168 group compared with the Model group. **B** Correlation heatmap of DEMs. Nodes represent individual metabolites. Line thickness indicates the absolute correlation coefficient (|r| > 0.5); red and blue lines represent positive and negative correlations, respectively. **C** Hierarchical clustering heatmap of DEMs. Red and blue indicate high and low expression levels, respectively. The color bar on the right represents the relative expression scale. **D** Volcano plot of

DEMs. Red and blue dots represent significantly upregulated and downregulated metabolites, respectively ($|\log_2 FC| \geq 1$, $P < 0.05$); gray dots indicate non-significant metabolites. **E**Scatter plot of mass-to-charge ratio (m/z) versus P-value. The vertical axis shows $-\log_{10}(P \text{ value})$, and the horizontal axis shows m/z. Red and blue dots denote significantly up- and downregulated metabolites, respectively (same thresholds as in D); gray dots represent non-significant metabolites. Dot size reflects the variable importance in projection (VIP) score.

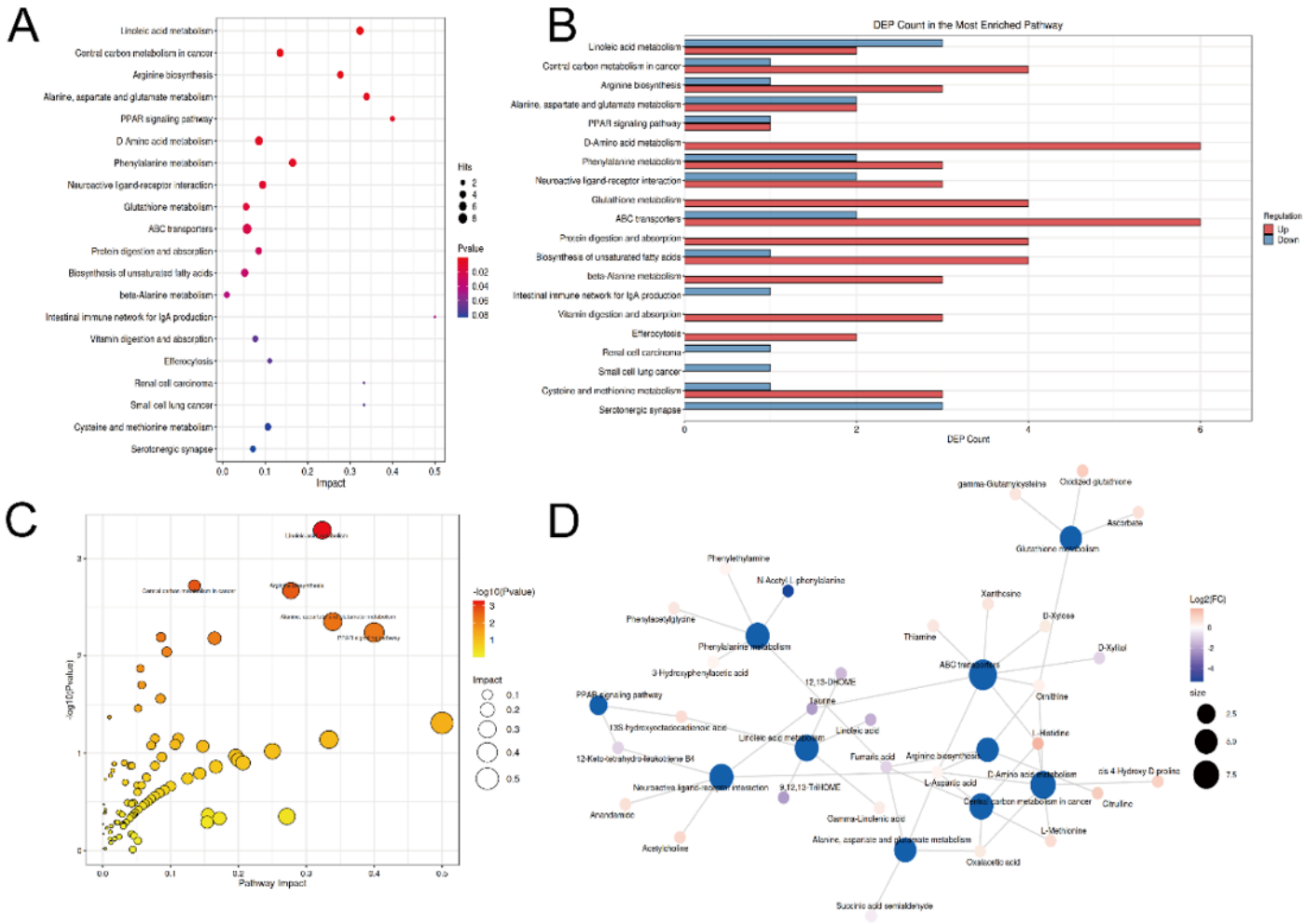


Figure 3

KEGG pathway enrichment and metabolic regulation network analysis. **A** KEGG enrichment bubble plot. The top 20 significant KEGG pathways are shown on the Y-axis. Bubble size indicates the number of enriched differential metabolites; color depth represents pathway significance (*P* value). **B** Bar chart of differential metabolite counts in KEGG pathways. Number of enriched differential metabolites in each of the top 20 pathways. **C** KEGG pathway enrichment scatter plot. Horizontal axis: pathway Impact value; vertical axis: $-\log_{10}(P \text{ value})$. Deeper color indicates smaller *P* value. Pathways closer to the upper right corner show more significant enrichment and greater impact. **D** Metabolite–KEGG pathway association network. Blue nodes represent pathways; other nodes represent metabolites. Pathway node size is

proportional to the number of associated metabolites. Metabolite node color indicates log_2FC (red: upregulation; blue: downregulation); deeper color reflects a greater degree of change.

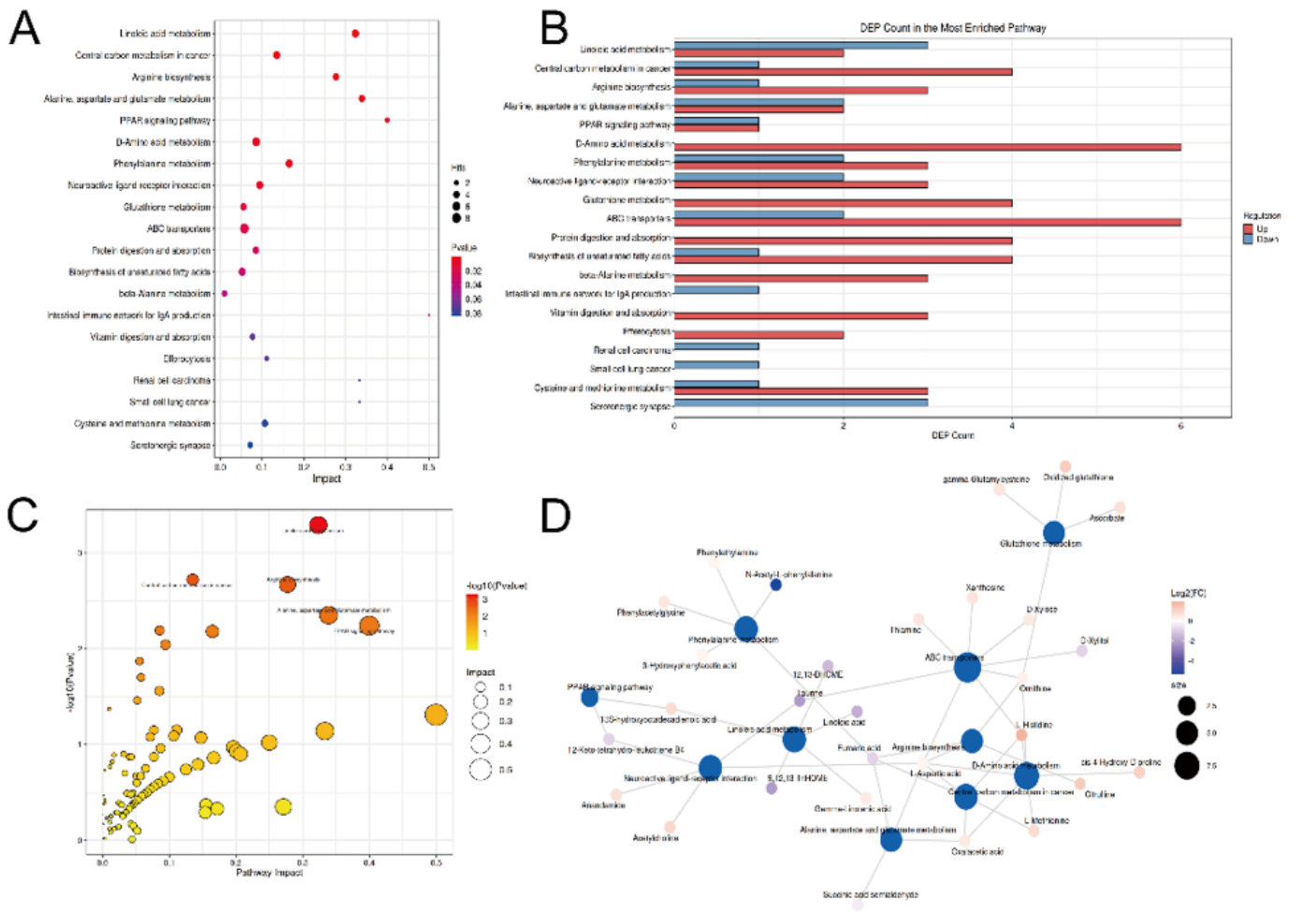


Figure 4

Differential protein expression profiles and functional enrichment analysis in a mouse model of CE following H-2-168 intervention. **A** Volcano plot of differentially expressed proteins (DEPs). Significantly upregulated (red) and downregulated (green) proteins are shown ($|log_2FC| > 1$, $P < 0.05$); blue dots indicate proteins with no significant difference. **B** Hierarchical clustering heatmap of DEPs. Expression patterns of DEPs between the H-2-168-treated group and the model group. Red: high expression; blue: low expression. **C–E**Enrichment bubble plots for Gene Ontology (GO) categories: Cellular Component (CC), Biological Process (BP), and Molecular Function (MF). The x-axis shows the enrichment ratio; the y-axis lists GO terms. Dot size reflects the number of DEPs; color intensity represents enrichment significance $-log_{10}$(*P*value). **F** Bar plot of KEGG pathway enrichment analysis. The x-axis shows the enrichment ratio; the y-axis lists KEGG pathways. Numbers on bars indicate the count of enriched DEPs; color intensity represents pathway significance (*P*value).

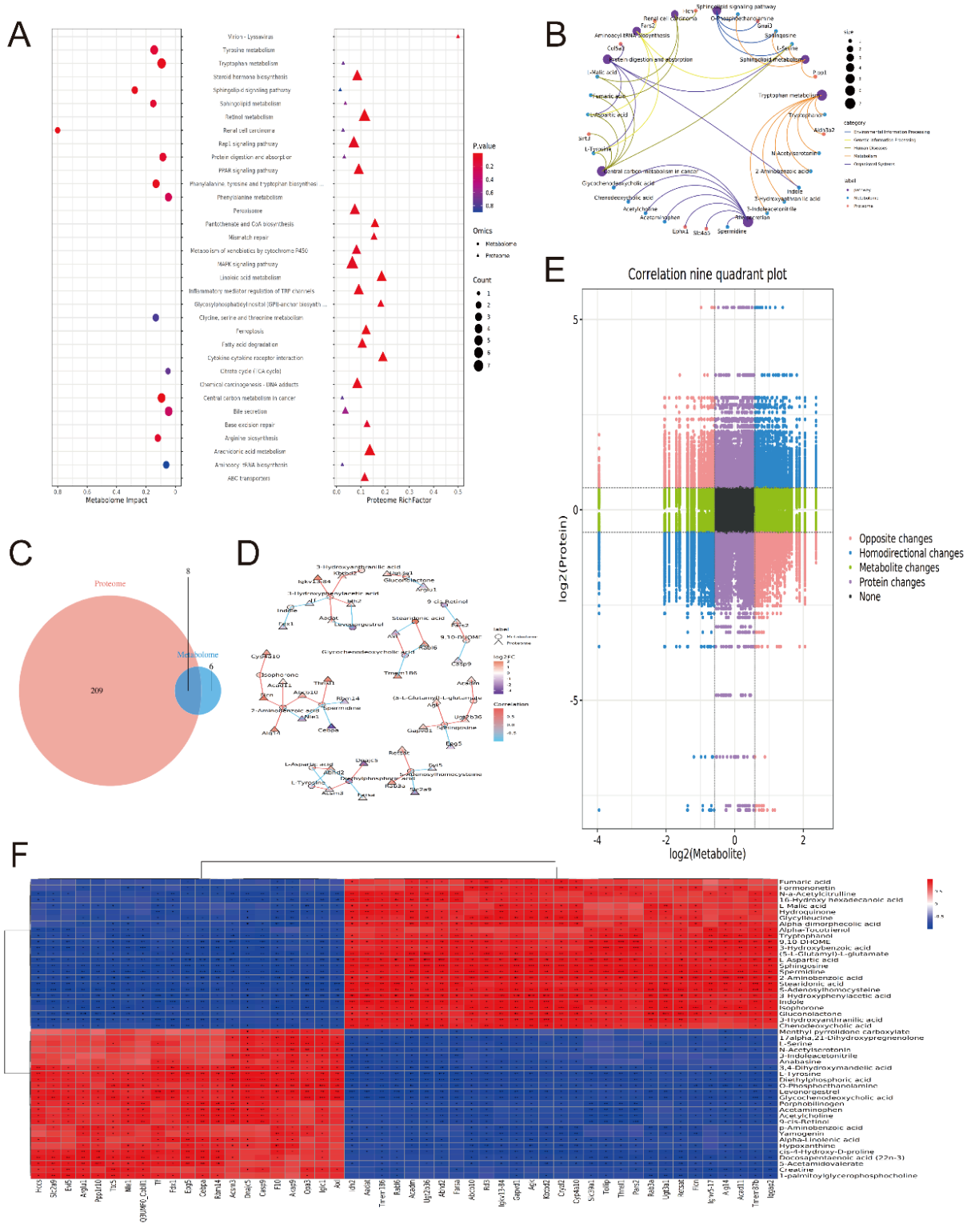


Figure 5

Integrated multi-omics analysis of differential molecules. A Pathway enrichment scatter plot for metabolomics (left, impact value) and proteomics (right, enrichment factor). Color: *P*value; point size: number of differential molecules per pathway. **B** KEGG interaction network. Nodes: metabolites and pathways (colors indicate pathway categories). Edges: associations between molecules and pathways. Node size reflects enrichment degree. **C** KEGG Venn diagram. Pink: proteome; blue: metabolome.

Overlap indicates common differential molecules. **D**Correlation network. Nodes: metabolites/proteins; edges: intermolecular interactions. Color gradient: $\log_2$FC; node size: significance $-\log_{10}$(*P*value). **E** Nine-quadrant association plot. Colors indicate change types: red, inverse; blue, parallel; green, metabolite-only; purple, protein-only; black, no significant change. **F** Clustered heatmap of differential molecules. Red: high expression; blue: low expression. Significance levels: *P*< 0.05, **P* < 0.01, ***P* < 0.001, ****P* < 0.0001.

Supplementary Files

This is a list of supplementary files associated with this preprint. Click to download.

- Graphicalabstractimage920300300DPI.png